RSC Advances

PAPER

View Article Online
View Journal | View Issue

Cite this: *RSC Adv.*, 2019, **9**, 9604

Design and fabrication of hydrotalcite-like ternary NiMgAl layered double hydroxide nanosheets as battery-type electrodes for high-performance supercapacitors

Chuan Jing,†[ab] Qiang Zhang,†[ab] Xiaoying Liu,*[a] Yuxiang Chen,[b] Xin Wang,[b] Luhao Xia,[b] Hao Zeng,[b] Decai Wang,[b] Wenzheng Zhang[b] and Fan Dong[c]

Received 22nd February 2019
Accepted 21st March 2019

DOI: 10.1039/c9ra01341e

rsc.li/rsc-advances

Hydrotalcite is an abundant mineral in nature and can be cost-effectively prepared in the laboratory, but there is almost no discussion about its application in the field of supercapacitors. Herein, hydrotalcite-like ternary NiMgAl LDHs with unique ultrathin nanosheets were designed and fabricated by a facile hydrothermal method. The preparation conditions, such as Ni/Mg molar ratio and hydrothermal reaction time, are evaluated carefully. The physical and chemical properties were also evaluated by various characterization techniques such as XRD, FIB/SEM, EDS, TEM, XPS and BET. The electrochemical behaviors of present samples were determined by CV, CC and cycling tests in a three-electrode system. As a battery-type electrode material in a supercapacitor, owing to the advantage of its unique layered structure, high specific area and obvious redox states, the fabricated Ni_2MgAl LDH-24 h nanosheets present an outstanding specific capacitance of 219.2 mA h g^{-1} at a current density of 1 A g^{-1} and superior cycling stability with 86.1% capacitance retention over 5000 cycles. Although 45.7% capacitance retention is not satisfactory when the current density increases from 1 to 3 A g^{-1} due to the NiMgAl LDH's low effective mass and conductivity, it is still a successful case for hydrotalcite application in supercapacitors by doping with Ni^{2+} to achieve high electrochemical performance. The design and fabrication strategy can facilitate the application of the natural hydrotalcite mineral in the energy storage field.

1. Introduction

The global energy crisis and worsening environmental issues resulting from the massive consumption of fossil fuels have attracted researchers' attention to study alternative clean energy sources. Currently, it is urgent to design and perfect safe, high-efficient, environmentally friendly and renewable clean energy storage devices. Compared with traditional dielectric capacitors, electrochemical capacitors, often called supercapacitors, have drawn a great deal of attention as a primary power source for this rising market due to their outstanding power density, cycling stability and rate performance.[1–5] Tremendous efforts have been made to design or develop supercapacitors, including using different nanomaterials and constructing various spatial structures to optimize the electrochemical performance. Transition metal oxides/hydroxides, *i.e.* NiO, $Ni(OH)_2$, Co_3O_4, $Co(OH)_2$, MnO_2, RuO_2 and their composites are commonly considered as promising electrode materials in supercapacitors because of their high capacitance as well as stable electrochemical properties.[6–10] However, the expensive cost of transition metal oxides/hydroxides materials hinders their large-scale practical application. Hence, developing novel materials with the merit of low cost and high performance becomes an urgent and challenging issue nowadays.

Layered double hydroxides (LDHs) is one kind of 2D layered materials.[11] LDHs take various combinations of metallic cationic and anionic species; the structural formula of LDHs is $[M_{1-x}^{2+}M_x^{3+}(OH)_2][A_{x/n}^{n-}\cdot mH_2O]$,[12] of which M^{2+} is divalent metallic cation (such as Mg^{2+}, Zn^{2+}, Ni^{2+}, *etc.*), M^{3+} is the trivalent metallic cation (such as Al^{3+}, Mn^{3+}, Co^{3+}, *etc.*) and A^{n-} is anion (such as Cl^-, OH^-, SO_4^{2-}, CO_3^{2-}, *etc.*) arranged in the interlayer. LDHs are commonly employed as adsorbents,[13] catalysis,[14,15] biological materials[16] and drug carrier.[17] Recently, LDHs have also attracted much attention for the potential

[a]*Chongqing Key Laboratory of Catalysis and New Environmental Materials, College of Environment and Resources, Chongqing Technology and Business University, Chongqing 400067, P. R. China. E-mail: lxy_ctbu@163.com; Fax: +86 23 65104131; Tel: +86 23 65104131*

[b]*State Key Laboratory of Mechanical Transmissions, College of Materials Science and Engineering, Chongqing University, Chongqing 400044, P. R. China*

[c]*Research Center for Environmental Science & Technology, Institute of Fundamental and Frontier Sciences, University of Electronic Science and Technology of China, Chengdu 611731, P. R. China*

† The authors are equally contributing to this manuscript.

application to battery-type supercapacitor because their layered structure possesses abundant channels to fabricate the intercalation/deintercalation of electrolyte ions and transition metallic elements with multiple redox states. Such structure can simultaneously make use of the merit of electrical double layered capacitance and faradaic capacity.[18] At present, a large amount of mature researches are related to LDH electrode materials, such as NiCo LDH,[19] NiMn LDH[20] and NiAl LDH.[21] However, there is almost no discussion of MgAl LDH (hydrotalcite), which is not only one of most natural abundant minerals but also a cost-effective materials prepared in the laboratory. The reason of no discussion could be that the elements of both Mg^{2+} and Al^{3+} are members of main group, which does not contribute to the electrochemical performance.

To solve this issue, two strategies can be considered. First, the electroactive element with obvious redox state is necessary for a boost of the pseudocapacitive performance. Second, the specific surface area of the materials should be as large as possible to supply a mass of active site to take part in faradaic redox reactions. As we know, nickel (Ni) is a transition metal element, and has obvious redox state (Ni^{2+}/Ni^{3+}) in electrochemical reaction.[22] Hence, a ternary LDH can be constructed by doping nickel into the hydrotalcite to meet the requirement of battery-type electrode materials. In addition, the classic hydrothermal method can be used to prepare the ternary LDH with large specific surface area.

In this work, we synthesized a novel NiMgAl LDH nanosheets *via* the facile one-pot hydrothermal technique. The preparation conditions of Ni/Mg molar ratio and hydrothermal reaction time were systematically evaluated. The high crystallinity and specific area of Ni_2MgAl LDH-24 h brought up an outstanding specific capacitance of 219.2 mA h g^{-1} at a current density of 1 A g^{-1} and eminent cycling performance of approximately 86.1% capacitance retention over 5000 cycles at a current density of 5 A g^{-1}. Although 45.7% capacitance retention is not satisfying while the current density increased from 1 to 3 A g^{-1} due to NiMgAl LDH's low effective mass and conductivity, it is still a successful case for hydrotalcite application in supercapacitor by doping the Ni^{2+} to achieve the electrochemical performance. The design and fabrication strategy can facilitate the application of natural hydrotalcite mineral in energy storage field.

2. Experimental section

2.1 Materials and chemical reagents

The chemical reagents for the preparation of electrode materials, such as $Ni(NO_3)_2\cdot 6H_2O$, $Mg(NO_3)_2\cdot 6H_2O$, $Al(NO_3)_2\cdot 9H_2O$ and urea, were purchased from Alfa Aesar (USA) without any further purification. Deionized water (18.2 MΩ) was used in this experiment. KOH was purchased Chongqing Chuandong Chemical Company (China).

2.2 Synthesis of NiMgAl LDHs

NiMgAl LDHs were fabricated by a facile hydrothermal method. $Ni(NO_3)_2\cdot 6H_2O$, $Mg(NO_3)_2\cdot 6H_2O$, $Al(NO_3)_3\cdot 9H_2O$ and urea were added into 70 mL deionized water. The feeding molar ratio of metal cations (Ni^{2+}, Mg^{2+} and Al^{3+}) *versus* urea is 3.3. The feeding contents of total metal cations were 4 mmol, of which the molar of bivalent metal cations was maintained at 3 mmol, and the molar ratios of Ni^{2+}/Mg^{2+} are kept at 1, 1.5 or 2. After ultrasonic stirring for 10 min, a clear mixing solution was obtained. Then, the aqueous solution was transferred into a 100 mL Teflon-lined stainless-steel autoclave. The hydrothermal process was conducted at 120 °C for 6, 12 or 24 h. The obtained green colloidal precipitate in the autoclave was washed with deionized water and ethanol for several times and dried at 60 °C for 10 h to obtain the NiMgAl LDH powder. Thus, the obtained samples were labelled according to the molar ratio of Ni^{2+}/Mg^{2+} and hydrothermal time, such as Ni_1MgAl LDH-6 h, $Ni_{1.5}$MgAl LDH-12 h, Ni_2MgAl LDH-24 h. It is worthy of mention that the urea served as a precipitator and anion provider for LDH in the nucleation growth process:[23]

$$CO(NH_3)_2 + 3H_2O \rightarrow 2OH^- + 2NH_4^+ + CO_2 \quad (1)$$

$$CO_2 + H_2O \rightarrow CO_3^- + 2H^+ \quad (2)$$

$$Ni^{2+} + Mg^{2+} + Al^{3+} + OH^- + CO_3^- \rightarrow NiMgAl\text{–}CO_3^{2-}\ LDH \quad (3)$$

2.3 Materials characterization

The crystallographic structure and phase composition of as-obtained samples were analyzed by the Rigaku D/max-2500 XRD using a Cu Kα radiation source (λ = 1.5406 Å). The morphological investigations of these samples were conducted by focused ion beam (Zeiss Auriga FIB/SEM) equipped with an energy dispersive X-ray spectrometer (EDS) attachment with an acceleration voltage of 5 kV. The lattice information on nanoscale was collected by high-resolution transmission electron microscopy (HRTEM, Zeiss Libra 200) with an acceleration voltage of 200 kV. Specific surface area and porosity of NiMgAl LDHs were determined by N_2 adsorption–desorption isotherms at 77 K using micromeritics Gemini VII. The information of chemical states was analyzed by the Thermo ESCALAB 250Xi X-ray photoelectron spectrometer (Al Kα, 1486.6 eV) at the scope range from 0 to 1350 eV.

2.4 Electrochemical measurements

The electrochemical behaviors were examined by electrochemical workstation (Chenhua, Shanghai) with the three-electrode system in 6 M KOH solution. The working electrode was assembled as follows: first, active materials, carbon black, and polyvinylidenefluoride (PVDF) were added to *N*-methyl-2-pyrrolidone (NMP) at a weight ratio of 7 : 2 : 1. Second, the mixture is ground continuously to form a uniform slurry. Third, the slurry was coated on nickel foam (1 × 1 cm^2) and dried in vacuum at 60 °C for 10 hours to obtain working electrodes. The active mass on the electrode is about 1.5–2 mg. Platinum foil (1 × 1 cm^2) was used as the counter electrode and saturated Hg/HgO electrode (SCE) as the reference electrode. The as-fabricated electrodes were characterized by the cyclic

voltammetry (CV) and galvanostatic charge–discharge (CC) method in the potential range from 0 to 0.4 V. The electrochemical impedance spectroscopy (EIS) was characterized at the frequency range of 100 kHz to 0.01 Hz with a disturbance voltage of 5 mV at the steady-state open-circuit potential. The specific capacity (C_s) of the samples was determined from CC process by the equation as follows:[24]

$$C_s = \frac{I \times \Delta t}{m} \quad (4)$$

where in C_s is the specific capacity (mA h g^{-1}), I is the discharge current (A), Δt is the discharge time (s) and m is the mass of active materials.

3. Results and discussion

3.1 Structure and morphology

NiMgAl LDHs were prepared by simple one-pot hydrothermal process. Urea served as the sources of alkali and intercalation anion by high temperature self-decomposition at hydrothermal system to facilitate the formation of LDH. The schematic synthesis route of NiMgAl LDH is presented in Scheme 1. XRD patterns of the NiMgAl LDH are demonstrated in the Fig. 1. All the NiMgAl LDHs present the strong reflections of LDH lattice with a series of (003) and (006) diffraction peaks at low angle indicating the formation of classical brucite-like crystal structure. The diffraction peaks at around 60° correspond to (110). No peak of other phase can be found, indicating the high purity of the as-synthesized NiMgAl LDHs. The lattice parameter $a = 2d_{110}$ is a function of average radii of the metal cations. The value of parameter a increases slightly as the feeding mole of Ni^{2+} increases, which can be ascribed to the larger radius of Ni^{2+} than Mg^{2+}. Interestingly, in both the peak density and peak area, the Ni_2MgAl LDH is apparently higher than Ni_1MgAl LDH and Ni_2MgAl LDH. Similarly, Ni_2MgAl LDH-24 h is apparently higher than Ni_2MgAl LDH-6 h and Ni_2MgAl LDH-12 h. The results suggest that the crystallinity increase with the increasing of reaction time and Ni/Mg molar ratio.

Fig. 2 presents the representative SEM images and corresponding EDS mapping of the as-synthesized samples at different reaction conditions. The NiMgAl LDHs are homogeneously grown without any aggregation, which can help to improve its electrochemical performance by increasing the number of exposed active atoms. In addition, the NiMgAl LDHs present dulcet nanosheet structure which also make a prominent contribution to electrochemical behavior by increasing the specific area and active site. Besides, abundant porous structure in NiMgAl LDHs nanosheets can be observed, which is favorable for enhancing the electrolyte diffusion and further enhancing supercapacitor performance. As can be seen from the Fig. 2a–e, no other morphologies can be found from the SEM images of these samples, which suggests the Ni^{2+} was inserted into the hydrotalcite crystal successfully during the hydrothermal reaction. The relevant EDS mapping of the typical Ni_2MgAl LDH-24 h (Fig. 2g–j) shows the homogeneous distribution of Ni, Mg, Al, O, clearly, indicating the effectiveness of the preparation method.

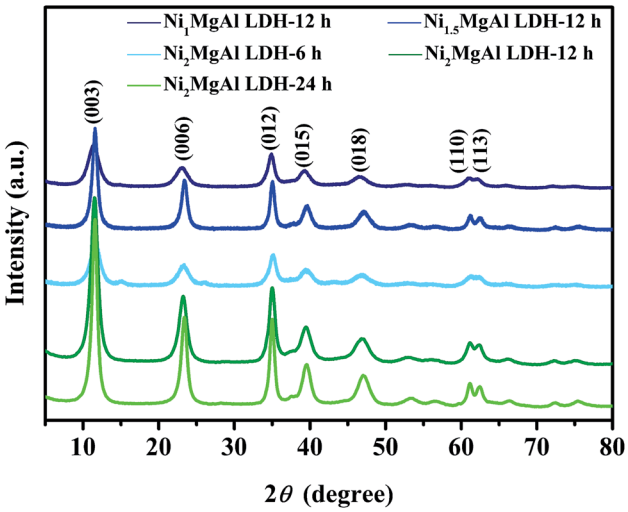

Fig. 1 XRD patterns of NiMgAl LDHs.

The ultrathin nanosheet structure of Ni_2MgAl LDH-24 h is further observed by the TEM (Fig. 3). As can be seen from Fig. 3a, the gossamer-like nanostructure exists in all over the Ni_2MgAl LDH-24 h nanosheets and the thickness of nanosheets is around 5 nm (Fig. 3b). The interplanar crystal spacings of 1.95 nm and 2.58 nm are on behalf of (018) and (012) plane of Ni_2MgAl LDH-24 h (Fig. 3c), respectively, which is in accordance with the XRD results.

To understand the chemical composition and valence state, the XPS measurement of the typical Ni_2MgAl LDH-24 h powder was conducted. As shown in Fig. 4a, the feature peaks of Ni 2p,

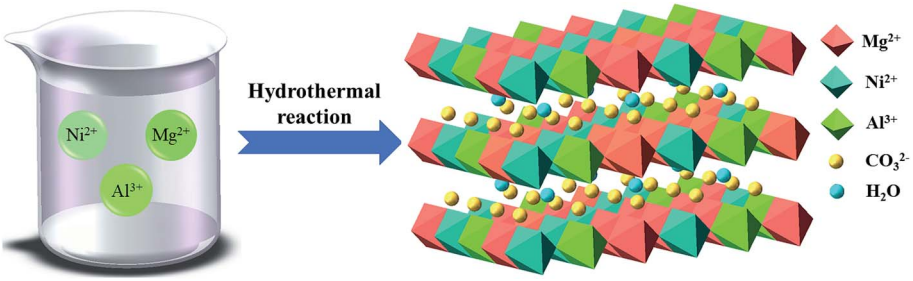

Scheme 1 Schematic drawing of formation mechanism of NiMgAl LDH by the hydrothermal method.

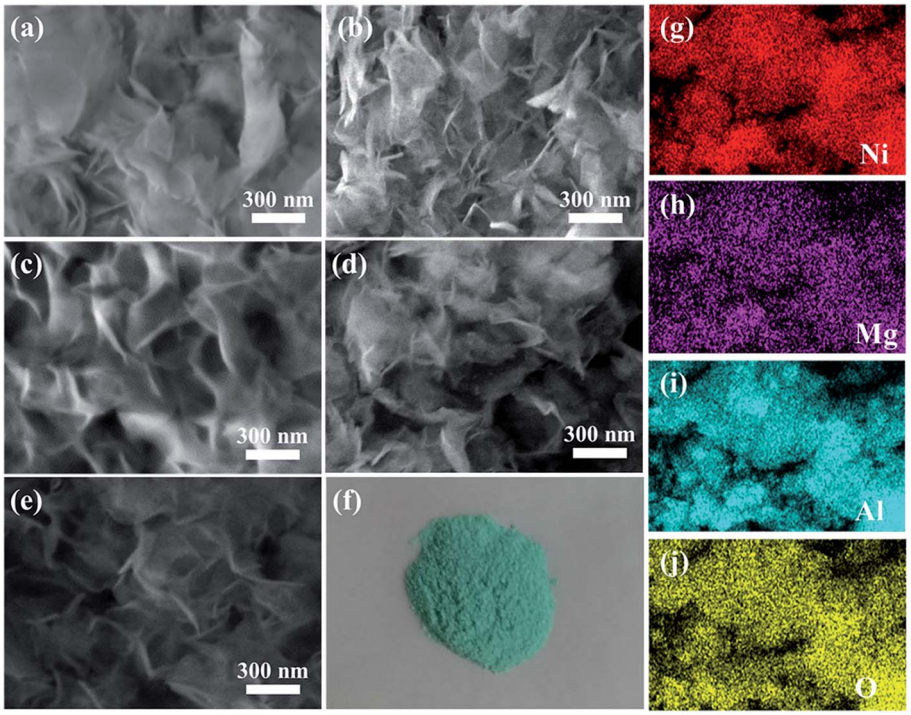

Fig. 2 SEM images of (a) Ni_1MgAl LDH-12 h, (b) $Ni_{1.5}MgAl$ LDH-12 h, (c) Ni_2MgAl LDH-12 h, (d) Ni_2MgAl LDH-6 h, (e) Ni_2MgAl LDH-24 h; (f) the photographic image of the Ni_2MgAl LDH-24 h; (g–j) the EDS mapping of Ni_2MgAl LDH-24 h.

Mg 1s, Al 2p, O 1s and C 1s are clearly found, suggesting the successful preparation of NiMgAl LDH. The peak of Ni 2p is separated to spin–orbit doublets and satellites (named "Sat."). Ni $2p_{3/2}$ peak is located at 855.7 eV and Ni $2p_{1/2}$ peak is located at 873.2 eV. The peaks at 851.6 and 879.7 eV are the "Sat. peaks" of Ni $2p_{3/2}$ and $2p_{1/2}$, respectively. No additional peak can be fitted in the spectrum indicating that only bivalent nickel ion in the crystal lattice of LDH exists. The results further suggest that the valence state of nickel ion does not change under hydrothermal process. Since magnesium and aluminum do not contribute to the electrochemical performance, they will not be analyzed here.

As we know, the high specific area can increase the contact chance between active material and electrolyte at solid–liquid interface. In addition, the high specific can also decrease the "dead volume" or "dead atoms" in electrode materials, which can facilitate the atomic or volume utilization.[25,26] Fig. 5 shows N_2 adsorption–desorption isotherms and pore-size distribution (inset) of representative Ni_2MgAl LDH with different hydrothermal time (6 h, 12 h and 24 h). All the adsorption isotherms display the type V characteristics with the obvious H3 hysteresis loops corresponding to the microporous and mesoporous structure in two-dimensional nanosheets.[27,28] The specific areas of Ni_2MgAl LDH-6 h, Ni_2MgAl LDH-12 h and Ni_2MgAl LDH-24 h are 67.33, 86.72 and 97.70 $m^2\ g^{-1}$, respectively. The result suggests that the specific surface area of LDH is increased by prolonging reaction time. The adsorption average pore diameter determined by the Brunauer–Emmett–Teller (BET) method of Ni_2MgAl LDH-6 h, Ni_2MgAl LDH-12 h and Ni_2MgAl LDH-24 h are 12.17, 14.09 and 14.43 nm, respectively. They are all within the mesoporous range, suggesting that it is beneficial to the intercalation/deintercalation of electrolyte ions. Overall, the Ni_2MgAl LDH-24 h possesses maximum specific area and mesoporous structure, which has great potential for electrochemical reaction.

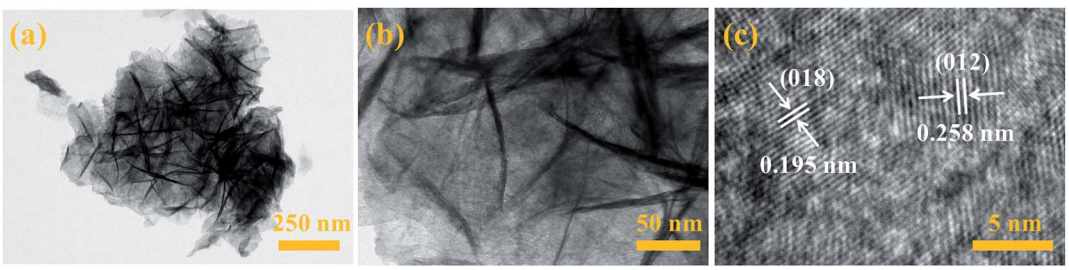

Fig. 3 TEM images of Ni_2MgAl LDH-24 h.

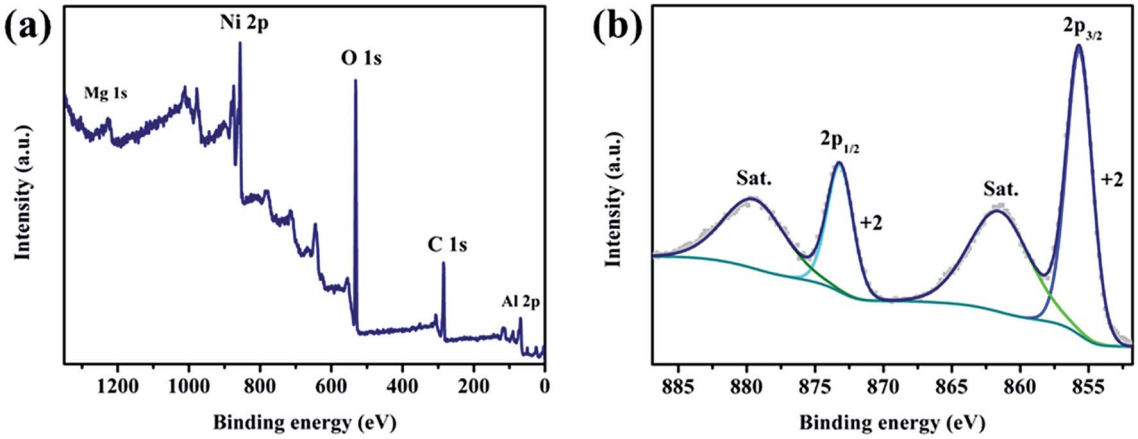

Fig. 4 XPS analysis of (a) the full spectrum, (b) the spectrum of Ni 2p of Ni_2MgAl LDH-24 h.

3.2. Electrochemical behavior

Electrochemical tests of the as-obtained electrode were conducted in three-electrode system. The effects of Ni/Mg molar ratio on NiMgAl LDH at the certain hydrothermal time (12 h) were characterized firstly by the CV and CC curves. As shown in Fig. 6a, the shapes of the CV curves displays the battery-type pseudocapacitive characteristics with a pair of faradic redox peaks corresponding to a reversible reaction:[29]

$$Ni(OH)_2 + OH^- \leftrightarrow NiOOH + H_2O + e^- \quad (5)$$

The cation of Mg^{2+} and Al^{3+} does not make contribution to the CV curves because there are no other valence states. This is the fundamental reason why hydrotalcite cannot be used in supercapacitors. Compared with integral area under the CV curves of remaining two samples, the integral area in the

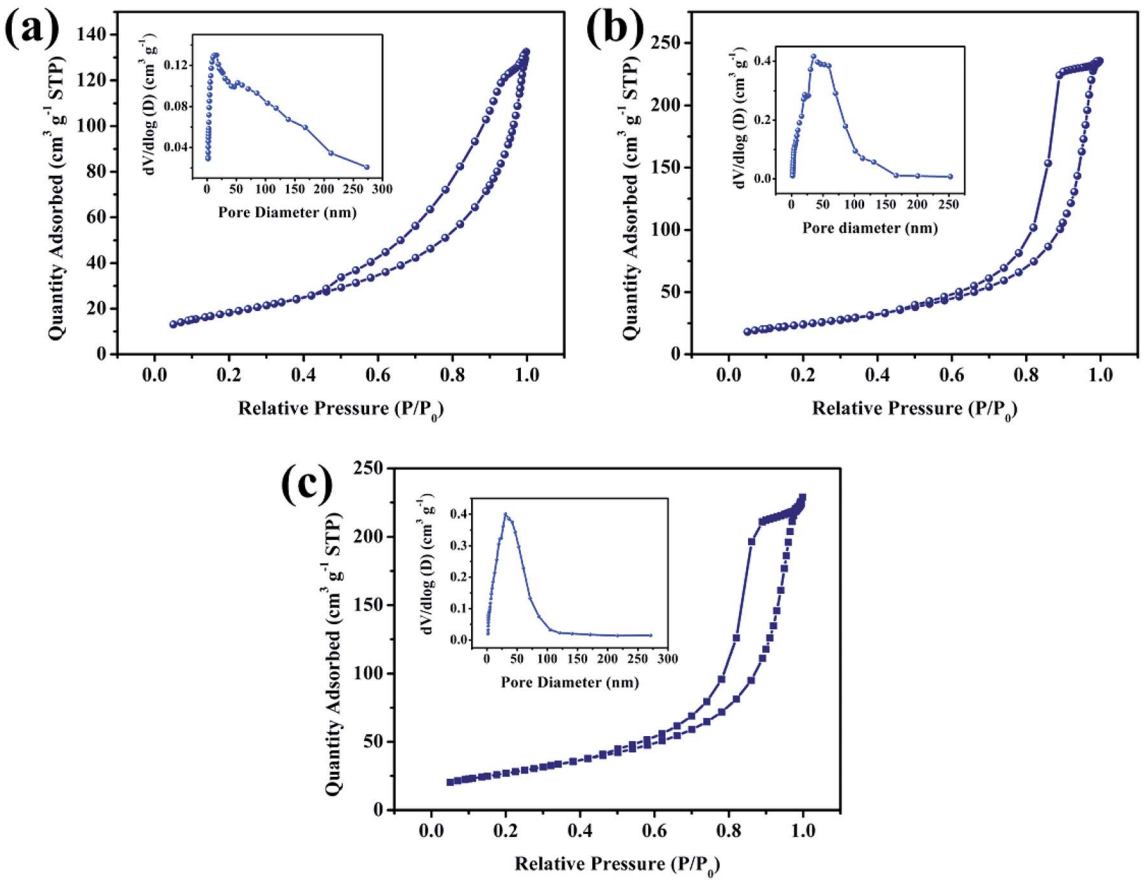

Fig. 5 N_2 adsorption–desorption isotherms and pore-size distribution (inset) of Ni_2MgAl LDH with different hydrothermal time, (a) 6 h, (b) 12 h, (c) 24 h.

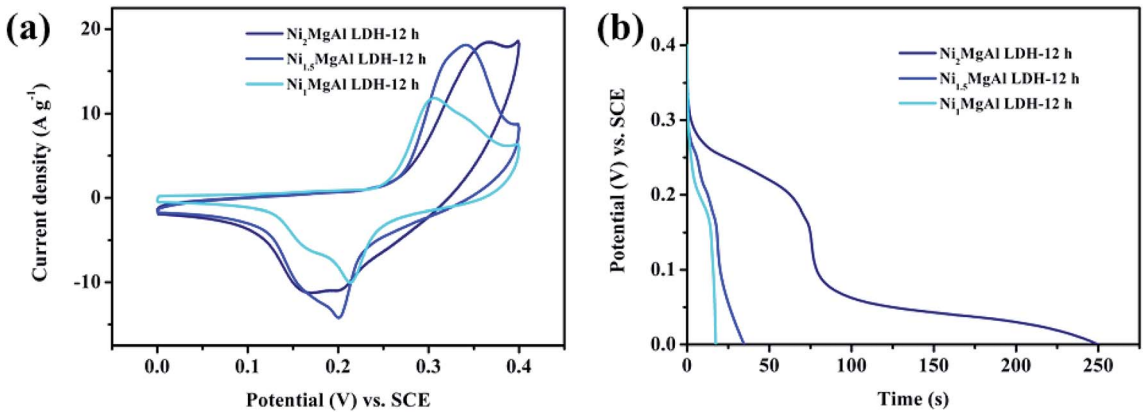

Fig. 6 The electrochemical performance measured in 6 M KOH solution. (a) CV curves of NiMgAl LDH-12 h with the different Ni/Mg molar ratio at a scan rate of 100 mV s^{-1}; (b) CC curves of NiMgAl LDH-12 h with the different Ni/Mg molar ratio at a current density of 2 A g^{-1}.

Ni_2MgAl LDH-12 h curve is the largest one due to the abundant amount of nickel in crystal lattice. It is well known that the specific capacitance is proportional to the integral area of the CV curve,[30] which means that the Ni_2MgAl LDH-24 h possesses a maximum capacitance. The result can be confirmed by the CC curves of three electrode at current density of 2 A g^{-1}. As shown in Fig. 6b, the nonlinear curves display the battery-type pseudocapacitive characteristics with obvious redox peak. The discharge time of Ni_2MgAl LDH-12 h is 249.6 s, longer than that of the $Ni_{1.5}MgAl$ LDH-12 h (34.6 s) and of Ni_1MgAl LDH-12 h (17.3 s). The corresponding specific capacitance of Ni_2MgAl LDH-12 h is 138.7 mA h g^{-1}, higher than that of the $Ni_{1.5}MgAl$ LDH-12 h (19.2 mA h g^{-1}) and of Ni_1MgAl LDH-12 h (9.6 mA h g^{-1}). The discharge time as well as specific capacitance of Ni_2MgAl LDH-12 h are nearly 7 times higher than those of $Ni_{1.5}MgAl$ LDH-12 h, and 14 times higher than those of

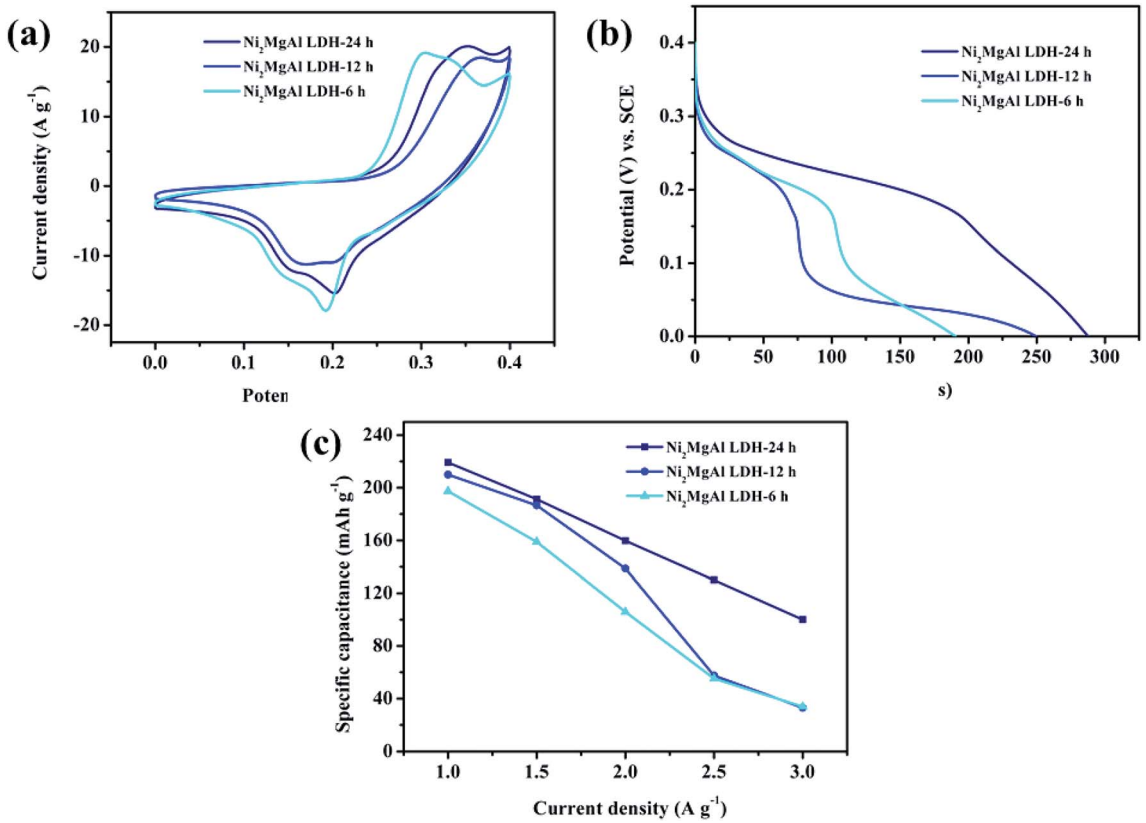

Fig. 7 The electrochemical performance measured in 6 M KOH solution. (a) CV curves of Ni_2MgAl LDH with different reaction time at a scan rate of 100 mV s^{-1}; (b) CC curves of the different reaction time at a current density of 2 A g^{-1}; (c) specific capacitances of NiMgAl LDH at different reaction time.

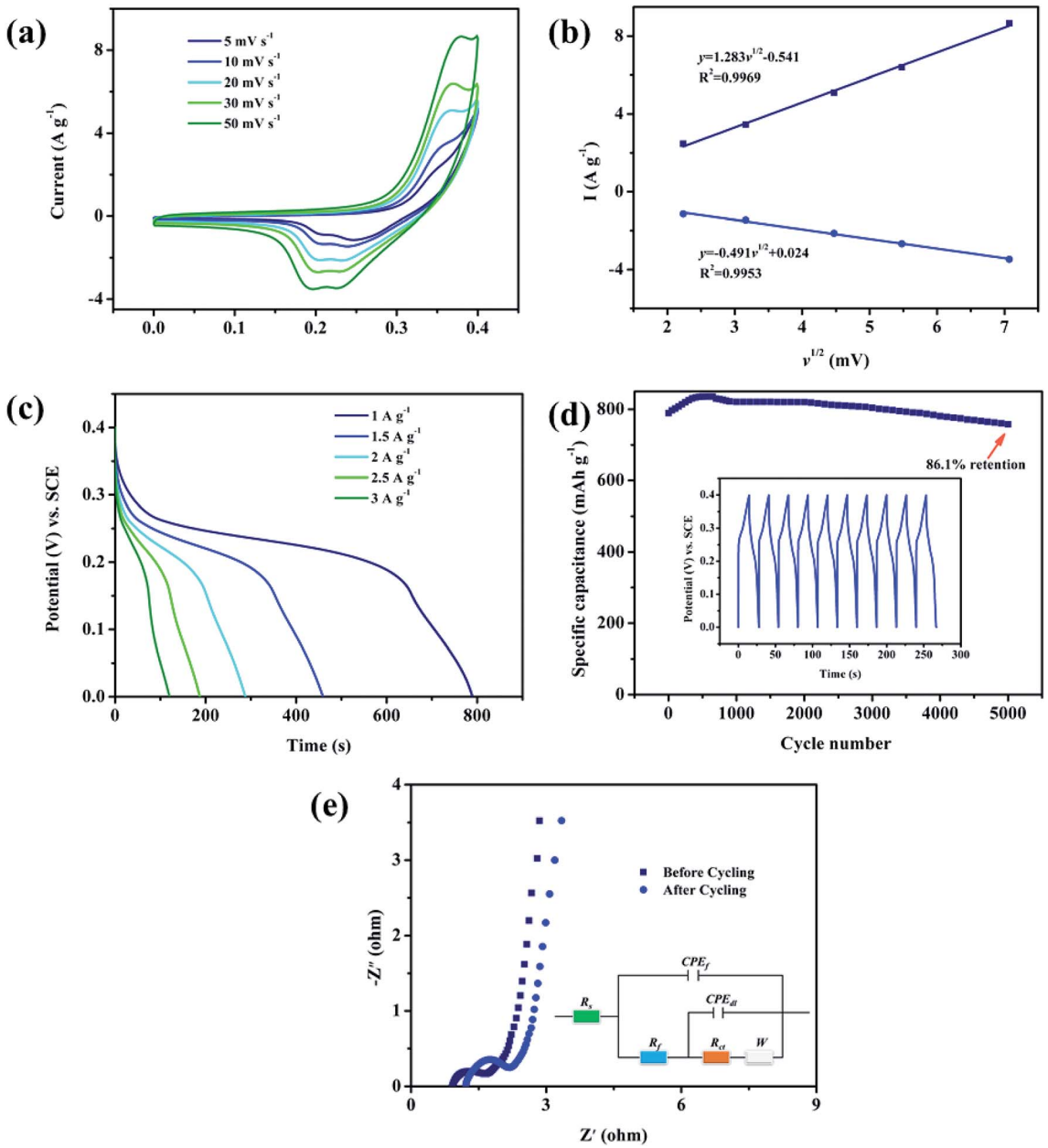

Fig. 8 (a) CV curves of Ni_2MgAl LDH-24 h at different scan rates; (b) linear relation between the anodic/cathodic peak currents and the square root of the scan rates; (c) CC curves of Ni_2MgAl LDH-24 h at different current densities ranging from 1 to 3 A g^{-1}; (d) cycling performance of Ni_2MgAl LDH-24 h at the current density of 5 A g^{-1}. The inset shows the charge–discharge curves of the last 10 cycles; (e) electrochemical impedance spectrum of Ni_2MgAl LDH-12 h at open circuit potential in the frequency range from 0.01 Hz to 100 kHz.

Ni_1MgAl LDH-12 h, suggesting that Ni^{2+} is an important element in these samples to improve their electrochemical performance, and the successful modification of hydrotalcite is an effective strategy to acquire pseudocapacitive characteristics. Hence, the test results show that the sample with the Ni/Mg molar ratio of 2 obtains superior pseudocapacitive performance. Consequently, the Ni/Mg molar ratio of 2 was selected as the criterion of sample preparation in subsequent experiments.

To obtain the best reaction condition, the electrochemical behaviors of Ni_2MgAl LDH with different reaction time are studied (Fig. 7). The CV curves of Ni_2MgAl LDH with different reaction time are shown in Fig. 7a. The integral area in CV curve for Ni_2MgAl LDH-24 h is the largest one among the three as-prepared samples, indicating that the optimal reaction time of 24 h is obtained. The CC curves of above samples at the constant current density of 2 A g^{-1} are presented in Fig. 7b. The Ni_2MgAl LDH-24 h presents the longest discharge time of these samples. According to eqn (4), the specific capacitances of Ni_2MgAl LDH-6 h, Ni_2MgAl LDH-12 h and Ni_2MgAl LDH-24 h are 105.9, 138.7, and 159.8 mA h g^{-1}, respectively, which is consistent with the results of CV curves. The plots of specific

capacitance *versus* different current densities are presented in Fig. 7c. The Ni_2MgAl LDH-24 h displays 45.7% retention rate when the current density changes from 1 to 3 A g-1, which is much better than 17.2% and 15.8% retention rates of Ni_2MgAl LDH-6 h and Ni_2MgAl LDH-12 h, respectively. However, the retention rates of these samples are slightly lower than those of reported nickel-based materials, such as $Ni(OH)_2$@carbon nanosheets,[31] $Ni(OH)_2$@carbon nanotubes,[32] NiO@carbon,[22] NiO.[33] The reasons could be as follows: (1) only the element of Ni^{2+} in NiMgAl LDH can take part in the pseudocapacitive behavior; (2) low conductivity of NiMgAl LDH results in greater diffusion resistance in intercalation or deintercalation process. In general, the Ni_2MgAl LDH-24 h delivers excellent capacitances, indicating that the optimal experimental condition is obtained.

In order to systematically evaluate the pseudocapacitive behavior of Ni_2MgAl LDH-24 h, a complete three-electrode test was performed. As shown in Fig. 8a obvious redox peaks appeared during the anodic and cathodic scanning, indicating the oxidation–reduction behavior of Ni^{+2}/Ni^{+3} according to the formula (5).[34] Notably, as the scanning rate increases, the integral area in CV curve increases gradually and the oxidation and reduction peaks move in the direction of the positive and negative potentials, respectively. The phenomenon is the result of diffusion resistance.[35] The CV plots are employed to determine the electrochemical reaction kinetics. The current (I) is a function of sweep rates (v), and the corresponding equation can be described as follows:[36]

$$I = av^b \quad (6)$$

wherein a and b are adjustable variables. If b is equal to 0.5, the redox reaction is controlled by the diffusion process; if b is equal to 1, the redox reaction is a surface-controlled process. From the Fig. 8b, there is a linear relationship with a high fitting degree (closing to 1) between I and $v^{1/2}$, suggesting that the diffusion-controlled intercalation/deintercalation is the main storage mechanism of Ni_2MgAl LDH-12 h.

The CC curves of Ni_2MgAl LDH-24 h are further measured to estimate its capacitive behaviors (Fig. 8c). The specific capacitance increases regularly with the decrease of current density. Especially, the specific capacitance of Ni_2MgAl LDH-24 h shows an excellent capacity which is up to 219.2 mA h g^{-1} at a current density of 1 A g^{-1}. Although the retention rate is not satisfying, it is still a successful battery-type electrode material for supercapacitor by using the modification of hydrotalcite. The measurement of CC was further conducted to assess the stability of as-prepared electrode at a current density of 5 A g^{-1} for 5000 cycles, as shown in Fig. 8d. Over 86.1% of original specific capacitance retention over 5000 cycles suggests outstanding cycling stability. The last ten symmetrical cycle curves illustrate that the structure of the electrode material was not damaged and maintained good coulombic efficiency. Fig. 8e presents the Nyquist plots of the Ni_2MgAl LDH-24 h before and after 5000 cycles. Equivalent circuit (R(Q(R(Q(RW))))) is used to fit the electrochemical impedance spectra.[37] The semicircle part at a high-frequency range with a linear part at the low-frequency range is found. The semicircle part is assigned to charge transfer resistance (R_{ct}), which is related to the transfer resistance of electron/ions and the linear part is assigned to Warburg impedance (W), which is related to the diffusion rate of the electrolyte ions on the solid–liquid interface. The intersection point between Nyquist plots and x-axis is assigned to solution resistance (R_s), which is related to the intrinsic resistance of the electrolyte.[38,39] The slightly lower slope of Ni_2MgAl LDH-24 h after cycling indicates that the cycling process has almost no effect on diffusion process of electrolyte ion. The solution resistance (R_s) increases from 0.95 Ω to 1.2 Ω, while the charge transfer resistance (R_{ct}) increases slightly from 1.1 Ω to 2.5 Ω, suggesting excellent cycling stability and durability.

4. Conclusion

Hydrotalcite is one of the natural minerals in nature, but it has no electrochemical properties and cannot be applied in the field of energy. In this paper, we have developed hydrotalcite-like ternary NiMgAl LDHs by a facile one-pot hydrothermal method. The experimental parameters have been carefully optimized by adjusting the Ni/Mg molar ratio and the hydrothermal reaction time. As a battery-type electrode material in supercapacitor, owing to the advantage of unique layered structure, high specific area and obvious redox states, the fabricated Ni_2MgAl LDH-24 h nanosheets deliver the outstanding specific capacitance of 219.2 mA h g^{-1} at a current density of 1 A g^{-1} and superior cycling stability of 86.1% capacitance retention over 5000 cycles. Although 45.7% capacitance retention is not satisfying while the current density increased from 1 to 3 A g^{-1}, it is still a successful case for hydrotalcite application in supercapacitor by doping the Ni^{2+} to achieve the high electrochemical performance. We believe that doping the Ni^{2+} may provide a new design and fabrication strategy to facilitate the application of natural hydrotalcite mineral in energy storage field.

Conflicts of interest

There are no conflicts to declare.

Acknowledgements

The authors gratefully acknowledge the financial support provided by the Graduate Research and innovation of Chongqing, China (Grant No. CYB18002), the National Natural Science Foundation of China (Grant No. 21576034), the Joint Funds of the National Natural Science Foundation of China-Guangdong (Grant No. U1801254), the State Education Ministry and Fundamental Research Funds for the Central Universities, China (106112017CDJXSYY0001, 2018CDYJSY0055, 106112017CDJQJ138802, 106112017CDJSK04XK11, and 2018CDQYCL0027), and the Innovative Research Team of Chongqing, China (CXTDG201602014). The authors also thank the Electron Microscopy Center of Chongqing University for materials characterizations. We specially appreciate Prof. Qian

Chen of Chongqing University greatly for her warm help in improving this article writing.

References

1 Q. Zhang, H. Chen, L. Luo, B. Zhao, H. Luo, X. Han, J. Wang, C. Wang, Y. Yang and T. Zhu, *Energy Environ. Sci.*, 2018, **11**, 669–681.
2 R. Patel, J. T. Park, M. Patel, J. K. Dash, E. B. Gowd, R. Karpoormath, A. Mishra, J. Kwak and J. H. Kim, *J. Mater. Chem. A*, 2018, **6**, 12–29.
3 W. Wei, X. Cui, W. Chen and D. G. Ivey, *Chem. Soc. Rev.*, 2011, **40**, 1697–1721.
4 H. Huang, W. Zhang, Y. Fu and W. Xin, *Electrochim. Acta*, 2015, **152**, 480–488.
5 Y. Wang, Z. Shi, Y. Huang, Y. Ma, C. Wang, M. Chen and Y. Chen, *J. Phys. Chem. C*, 2009, **113**, 13103–13107.
6 H. Chen, B. Zhang, F. Li, M. Kuang, M. Huang, Y. Yang and Y. X. Zhang, *Electrochim. Acta*, 2016, **187**, 488–495.
7 K. Tao, P. Li, L. Kang, X. Li, Q. Zhou, L. Dong and W. Liang, *J. Power Sources*, 2015, **293**, 23–32.
8 Q. Zhang, Z. Liu, B. Zhao, Y. Cheng, L. Zhang, H.-H. Wu, M.-S. Wang, S. Dai, K. Zhang and D. Ding, *Energy Storage Materials*, 2018.
9 G. A. Snook, P. Kao and A. S. Best, *J. Power Sources*, 2011, **196**, 1–12.
10 J. Li and H. Xie, *Mater. Lett.*, 2012, **78**, 106–109.
11 M. Shao, F. Ning, Y. Zhao, J. Zhao, M. Wei, D. G. Evans and X. Duan, *Chem. Mater.*, 2012, **24**, 1192–1197.
12 S. Casenave, H. Martinez, C. Guimon, A. Auroux, V. Hulea, A. Cordoneanu and E. Dumitriu, *Thermochim. Acta*, 2001, **379**, 85–93.
13 K. Gupta, J.-B. Huo, J.-C. E. Yang, M.-L. Fu, B. Yuan and Z. Chen, *Chem. Eng. J.*, 2019, **355**, 637–649.
14 B. Sels, D. De Vos, M. Buntinx, F. Pierard, A. Kirsch-De Mesmaeker and P. Jacobs, *Nature*, 1999, **400**, 855.
15 G. Fan, F. Li, D. G. Evans and X. Duan, *Chem. Soc. Rev.*, 2014, **43**, 7040–7066.
16 H. B. Yao, Z. H. Tan, H. Y. Fang and S. H. Yu, *Angew. Chem., Int. Ed.*, 2010, **49**, 10127–10131.
17 A. Alcantara, P. Aranda, M. Darder and E. Ruiz-Hitzky, *J. Mater. Chem.*, 2010, **20**, 9495–9504.
18 X. Cao, H.-Y. Zeng, S. Xu, J. Yuan, J. Han and G.-F. Xiao, *Appl. Clay Sci.*, 2019, **168**, 175–183.
19 X. Cai, X. Shen, L. Ma, Z. Ji, C. Xu and A. Yuan, *Chem. Eng. J.*, 2015, **268**, 251–259.
20 Y. Yuan, J. Zhou, M. I. Rafiq, S. Dai, J. Tang and W. Tang, *Electrochim. Acta*, 2019, **295**, 82–91.
21 X. Hua, C.-J. Mao, J.-S. Chen, P.-P. Chen and C.-F. Zhang, *J. Alloys Compd.*, 2019, **777**, 749–758.
22 T. Liu, L. Zhang, B. Cheng, W. You and J. Yu, *Chem. Commun.*, 2018, **54**, 3731–3734.
23 X. L. Guo, X. Y. Liu, X. D. Hao, S. J. Zhu, F. Dong, Z. Q. Wen and Y. X. Zhang, *Electrochim. Acta*, 2016, **194**, 179–186.
24 Y. Fan, Z. Ma, L. Wang, Y. Dong, T. Jiang, Z. Li, L. Liu and G. Shao, *Electrochim. Acta*, 2018, **269**, 62–69.
25 P. Bandyopadhyay, X. Li, N. H. Kim and J. H. Lee, *Chem. Eng. J.*, 2018, **353**, 824–838.
26 L. Liu, T. Guan, L. Fang, F. Wu, Y. Lu, H. Luo, X. Song, M. Zhou, B. Hu and D. Wei, *J. Alloys Compd.*, 2018, **763**, 926–934.
27 I. B. Saïd, K. Sadouki, S. Masse, T. Coradin, L. S. Smiri and S. Fessi, *Microporous Mesoporous Mater.*, 2018, **260**, 93–101.
28 G. Zhang, S. Xiu, Y. Wei, Q. Zhang and K. Cai, *CrystEngComm*, 2018, **20**, 4364–4369.
29 H. Peng, C. Jing, J. Chen, D. Jiang, X. Liu, B. Dong, F. Dong, S. Li and Y. Zhang, *CrystEngComm*, 2019, **21**, 470–477.
30 J.-H. Zhong, A.-L. Wang, G.-R. Li, J.-W. Wang, Y.-N. Ou and Y.-X. Tong, *J. Mater. Chem.*, 2012, **22**, 5656–5665.
31 M. Xie, Z. Xu, S. Duan, Z. Tian, Y. Zhang, K. Xiang, M. Lin, X. Guo and W. Ding, *Nano Res.*, 2018, **11**, 216–224.
32 Q. Qin, J. Liu, W. Mao, C. Xu, B. Lan, Y. Wang, Y. Zhang, J. Yan and Y. Wu, *Nanoscale*, 2018, **10**, 7377–7381.
33 G. S. Gund, C. D. Lokhande and H. S. Park, *J. Alloys Compd.*, 2018, **741**, 549–556.
34 Z. Tang, C. h. Tang and H. Gong, *Adv. Funct. Mater.*, 2012, **22**, 1272–1278.
35 S. Li, W. Huang, Y. Yang, J. Ulstrup, L. Ci, J. Zhang, J. Lou and P. Si, *J. Mater. Chem. A*, 2018, **6**, 20480–20490.
36 H. Liang, J. Lin, H. Jia, S. Chen, J. Qi, J. Cao, T. Lin, W. Fei and J. Feng, *J. Power Sources*, 2018, **378**, 248–254.
37 C. Jing, Z. Wang, Y. Gong, H. Huang, Y. Ma, H. Xie, H. Li, S. Zhang and F. Gao, *Corros. Sci.*, 2018, **138**, 353–371.
38 C. Jing, X. Liu, X. Liu, D. Jiang, B. Dong, F. Dong, J. Wang, N. Li, T. Lan and Y. Zhang, *CrystEngComm*, 2018, **20**, 7428–7434.
39 Y. Zhao, X. He, R. Chen, Q. Liu, J. Liu, J. Yu, J. Li, H. Zhang, H. Dong and M. Zhang, *Chem. Eng. J.*, 2018, **352**, 29–38.